




Estimating integrated information in bidirectional neuron-astrocyte communicationLuis Abrego ¹, Susanna Gordleeva ^{2,3}, Oleg Kanakov,³ Mikhail Krivonosov ³ and Alexey Zaikin^{1,3,4,5,*}¹*Department of Mathematics, University College London, London, United Kingdom*²*Neuroscience and Cognitive Technology Laboratory, Center for Technologies in Robotics and Mechatronics Components, Innopolis University, Innopolis, Russia*³*Lobachevsky State University of Nizhny Novgorod, Nizhny Novgorod, Russia*⁴*Institute for Women's Health, University College London, London WC1E 6BT, United Kingdom*⁵*Centre for Analysis of Complex Systems, Sechenov First Moscow State Medical University (Sechenov University), Moscow, Russia*

(Received 24 August 2020; accepted 4 January 2021; published 19 February 2021)

There is growing evidence that suggests the importance of astrocytes as elements for neural information processing through the modulation of synaptic transmission. A key aspect of this problem is understanding the impact of astrocytes in the information carried by compound events in neurons across time. In this paper, we investigate how the astrocytes participate in the information integrated by individual neurons in an ensemble through the measurement of “integrated information.” We propose a computational model that considers bidirectional communication between astrocytes and neurons through glutamate-induced calcium signaling. Our model highlights the role of astrocytes in information processing through dynamical coordination. Our findings suggest that the astrocytic feedback promotes synergetic influences in the neural communication, which is maximized when there is a balance between excess correlation and spontaneous spiking activity. The results were further linked with additional measures such as net synergy and mutual information. This result reinforces the idea that astrocytes have integrative properties in communication among neurons.

DOI: [10.1103/PhysRevE.103.022410](https://doi.org/10.1103/PhysRevE.103.022410)**I. INTRODUCTION**

Traditionally, it was thought that astrocytic regulation was only supportive for structural and metabolic processes in the neurons [1]. Recent studies provide evidence about the role of astrocytes as signaling cells in the brain [1–6]. It is found that astrocytes and neurons have specific and varied communication pathways through release of transmitters in which they can interact in a bidirectional manner. In particular, accumulated results demonstrate that astrocytes respond mainly with Ca^{2+} elevations to excitatory neuronal activity mediated by metabotropic glutamate receptors (mGluRs) [7]. As a response, astrocytes release molecules also known as gliotransmitters, which feed back onto the synaptic cleft [8]. This promotes the activity of presynaptic and postsynaptic neurons allowing the modulation of excitatory and inhibitory transmission [9]. Furthermore, Ca^{2+} signals can propagate to neighboring astrocytes as an intercellular Ca^{2+} wave involving several cells [3,10–14]. Thus, the different pathways have different functional roles in neural communication.

This mechanism hints about the deep implications of astrocytes in the synaptic information transfer. Ongoing research shows that astrocytic signaling promotes dynamical synchronization of firing, integration of signals from different synaptic pathways, and modulation of neuronal transmission [4,10,12,15,16]. Interestingly, it is suggested that the astrocyte-dependent dynamics allows neuronal groups to be

linked at different degrees of complexity, promoting systemic integration of neural networks [10,17–19]. This is fundamental for cognitive and behavioral functions, as they are thought to emerge from the dynamical coordination between different brain areas. Thus, it comes as no surprise that there is a long-standing interest in understanding information processing through astrocytic signaling.

The integrated information theory (IIT) provides a mathematical framework using information-theoretic principles, that formulate the information generated from a whole system through its transition dynamics, more and beyond than the sum of its parts [20–22]. Ongoing evidence provides insights about the practical applications of this measure: it has been used to estimate information generated in the brain to understand the basis of consciousness [23–25] but its different mathematical descriptions have been adopted also as quantitative measure of dynamical complexity in many-body systems [26–29]. This is the degree of causal interconnection of the different parts of a system in terms of the overall information exchange. Our aim is understanding conditions in which integrated information arises from the bidirectional communication in neuron-astrocyte ensembles.

In this paper, we extend observations from our previous work about neuron-astrocytic networks [28] by including glutamate-induced calcium signaling [10,12,13,15,30]. This model considers the process of glutamate being released from excitatory neurons to produce IP_3 through activation of phosphoinositide-specific phospholipase C- β (PLC β) followed by the IP_3 -dependent Ca^{2+} -induced Ca^{2+} -release

*alexey.zaikin@ucl.ac.uk

mechanism. Synaptic modulation is modeled by the action of astrocytes through Ca^{2+} pulses and oscillations, and astrocytic communication is established through Ca^{2+} and IP_3 diffusion mediated by gap junction channels.

Using simulations, we calculate integrated information using a small neuroastrocytic network under different conditions to relate our estimations with the anatomical connectivity, dynamics, and noise levels of the ensembles. We provide evidence which shows that astrocytes have a role in increasing integrated information. More specific, the quantity grows as the neuron-astrocyte feedback is reinforced. In this case, there is an enhancement of synaptic transmission and dynamic coordination in neurons due to the stimulation of calcium events mediated by glutamate patterns.

Next, integrated information seems to be enhanced for less densely connected networks. In our results, nearest-neighbor coupling is favored over full connectivity. This implies that higher dynamical complexity could be reached from local interactions enabling the system to have more segregated dynamics. Simultaneously, integration of information could be obtained through joint influence from astrocytes and neighboring neurons.

We also simulate Ca^{2+} oscillatory signaling studied in [28], where synaptic feedback to astrocytes was neglected. The comparison of results strongly suggests that bidirectional neuron-astrocyte communication shows (in all cases) considerably higher activity-dependent integrated information at given neural dynamics and connectivity. This means that influence from astrocytes alone is not enough to increase the integration of information and a feedback from neurons is needed. Overall, these results suggest that the astrocytic control may enhance the dynamical complexity in synaptic information processing through bidirectional coupling.

II. METHODS AND MODEL

A. Neuron model and neuron-astrocyte interaction

This work estimates integrated information generated through glutamate-mediated neuron-astrocyte signaling. First, neuronal dynamics is implemented using the Hodgkin-Huxley model [31] with a network of six coupled neurons seeded in a square lattice, connected by using both all-to-all and nearest-neighbor couplings. We also consider different neuronal schemes altering the excitatory and inhibitory balance. Therefore, to understand the interplay of the synaptic inputs arranged with different couplings, we consider three main schemes: (1) six excitatory neurons connected all-to-all (denoted in this work as exc-full), (2) six excitatory neurons connected by nearest-neighbor coupling (exc-nns), and (3) one inhibitory and five excitatory neurons allocated in the square, all connected by nearest-neighbor coupling (inh-nns).

A schematic description of the studied networks is shown in Fig. 1. The membrane potential $V^{(i)}$ of each neuron i is described by the equation

$$C_m \frac{dV^{(i)}}{dt} = I_{\text{channel}}^{(i)} + I_{\text{app}}^{(i)} + \sum_j I_{\text{syn}}^{(ij)} + I_{\text{ext}}^{(i)}, \quad (1)$$

where the sum over j contains inputs from presynaptic neurons connected synaptically to the i th neuron as described

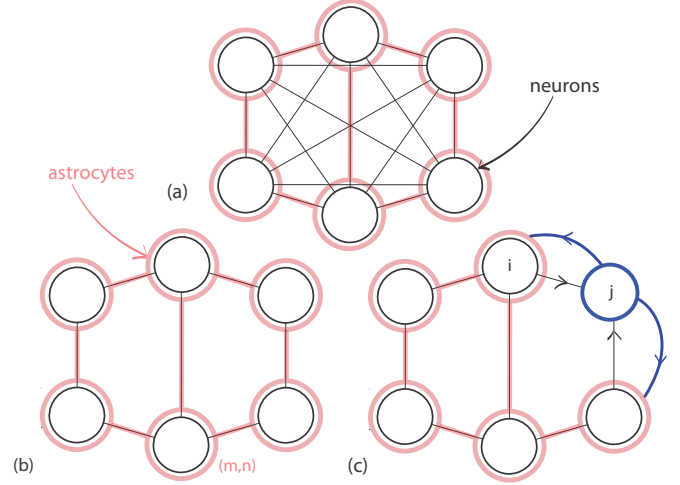


FIG. 1. Neuron-astrocytic networks: (a) six excitatory neurons connected all-to-all (exc-full), (b) six excitatory neurons connected by nearest neighbors (exc-nns), (c) one inhibitory neuron and five excitatory neurons connected by nearest neighbors (inh-nns). Connections without arrows are bidirectional. Astrocytes are associated to a single excitatory neuron and are connected between themselves through nearest-neighbor coupling. In (c) the inhibitory neuron is not linked to an astrocyte.

below. Time in neuronal dynamics is measured in ms; C_m is the specific membrane capacitance, measured in $\mu\text{F}/\text{cm}^2$. Ionic currents (for the sodium, potassium, and leak channels, respectively) measured in $\mu\text{A}/\text{cm}^2$ are expressed as

$$I_{\text{channel}} = -g_{Na}m^3h(V - E_{Na}) - g_Kn^4(V - E_K) - g_l(V - E_l),$$

$$\frac{dx}{dt} = \alpha_x(1 - x) - \beta_x x, \quad x = m, n, h \quad (2)$$

where m and h are the activation and inactivation variables of the sodium current and n the activation variable of the potassium current. Nonlinear gating functions α_x and β_x are defined by the original Hodgkin-Huxley model with the membrane potential shifted by 65 mV. The parameters g_{Na} , g_K and g_l are the maximum conductances (measured in mS/cm^2) related to the ion channels, and E_{Na} , E_K , and E_l are their corresponding reversal potentials. In this paper, we use the following parameters: $E_{Na} = 55$ mV, $E_K = -77$ mV, $E_l = -54.4$ mV, $g_{Na} = 120$ mS/cm^2 , $g_K = 36$ mS/cm^2 , $g_l = 0.3$ mS/cm^2 , and $C_m = 1$ $\mu\text{F}/\text{cm}^2$.

The applied current $I_{\text{app}}^{(i)}$ determines the dynamical regime of an autonomous neuron, which can be oscillatory, bistable, or excitable. We choose the excitable regime with $I_{\text{app}}^{(i)} = -5.0$ $\mu\text{A}/\text{cm}^2$ [32,33].

The current $I_{\text{syn}}^{(ij)}$ introduced in [28] reflects the synapse at neuron i due to the input from presynaptic neuron j and is defined as

$$I_{\text{syn}}^{(ij)} = \frac{g_{\text{syn,eff}}(V^{(j)} - E_{\text{syn},i})}{1 + \exp\left[-\frac{(V^{(i)} - \theta_{\text{syn}})}{k_{\text{syn}}}\right]}, \quad (3)$$

where parameter $g_{\text{syn,eff}}$ quantifies the synaptic weight and incorporates the astrocyte modulation due to release of

gliotransmitters in the neuron-astrocyte network as described in Eq. (9). The reversal potential is $E_{\text{syn}} = -90$ mV for the inhibitory synapse and $E_{\text{syn}} = 0$ mV for the excitatory one. Parameters $\theta_{\text{syn}} = 0$ mV and $k_{\text{syn}} = 0.2$ mV determine the midpoint of the synaptic activation or inactivation sigmoid and its steepness. Finally, each neuron receives an external input $I_{\text{ext}}^{(i)}$ defined as a Poisson pulse train with mean rate λ . The pulse shape is square with constant duration of 10 ms, and amplitudes sampled independently from a uniform distribution in $[-1.8, 1.8]$. Each pulse train is generated independently for each neuron.

Astrocytes along with presynaptic and postsynaptic neurons interact through the so-called tripartite synapse [9]. Neurotransmitters (such as glutamate) are released from the presynaptic neuron and bound to the astrocytic receptors activating signaling pathways that influence the synaptic transmission. Numerous observations indicate that active astrocytes release gliotransmitters in a Ca^{2+} -dependent manner through a process known as calcium-induced calcium release (CICR). When the neurotransmitters interact with the mGluRs, inositol 1,4,5-trisphosphate (IP_3) channels are activated. Next, IP_3 binds available receptors at the endoplasmic reticulum (ER) IP_3 Rs resulting in a Ca^{2+} influx from ER to the cytosolic volume. This increase in cytosolic Ca^{2+} leads to the release of gliotransmitters into the synaptic cleft. These gliotransmitters are uptaken by the presynaptic and postsynaptic neurons (this process may even include diffusion towards neighboring astrocytes and the extra-synaptical space) causing different forms of potentiation or inhibition in synaptic transmission [34].

The concentration of the neurotransmitter (glutamate) released from the synapse at neuron i is quantified by a dimensionless variable $G^{(i)}$ [19], whose dynamics is described by

$$\frac{dG^{(i)}}{dt} = -\alpha_G G^{(i)} + \frac{\beta_G}{1 + \exp(-V^{(i)}/V_G)}, \quad (4)$$

where $\alpha_G = 32$ and $\beta_G = 295$ denote the relaxation and production rates of glutamate, $V_G = 0.5$ mV. In the case of excitatory synapses, glutamate is stored and released due to the action potential.

Glutamate released from presynaptic neurons is integrated over a larger timescale by the IP_3 dynamics through J_G , Eq. (6). With the increase of presynaptic firing rate modulated by J_G the amplitude of IP_3 promotes spontaneous calcium oscillations through the Andronov-Hopf bifurcation [35]. These oscillations disappear in the low resting state and at high concentrations of IP_3 . In this work, for fixed α_G and β_G the neuronal firing frequency can be modulated through the Poisson input frequency and the astrocytic feedback by g_s introduced in (9). In particular, as it will be described later, by defining a fixed input frequency the parameter g_s will tune the feedback from the astrocytes to neurons. The range in which spontaneous calcium activity appears will be defined by the joint dynamics of the neuron-astrocyte network.

B. Astrocytic dynamics and feedback

The astrocyte dynamics is described through the CICR process [13] as follows:

$$\begin{aligned} \frac{d\text{Ca}^{(m)}}{dt} &= J_{\text{ER}}^{(m)} - J_{\text{pump}}^{(m)} + J_l^{(m)} + J_{\text{in}}^{(m)} - J_{\text{out}}^{(m)} + J_{\text{Ca,diff}}^{(m)}, \\ \frac{d\text{IP}_3^{(m)}}{dt} &= \frac{\text{IP}_3^* - \text{IP}_3^{(m)}}{\tau_{\text{IP}_3}} + J_{\text{PLC}}^{(m)} + J_{\text{Glu}}^{(m)} + J_{\text{IP}_3,\text{diff}}^{(m)}, \\ \frac{dh^{(m)}}{dt} &= a_2 \left[d_2 \frac{\text{IP}_3^{(m)} + d_1}{\text{IP}_3^{(m)} + d_3} (1 - h^{(m)}) - \text{Ca}^{(m)} h^{(m)} \right], \end{aligned} \quad (5)$$

where $\mathbf{m} = (m, n)$ defines the location of each astrocyte in a square lattice, $m = 1, 2, 3$ and $n = 1, 2$.

The Ca^{2+} equation expresses the calcium fluxes in the astrocyte through different channels. J_{pump} denotes the flux via the ATP-dependent pump from the cytoplasm to ER, J_{ER} models the flux from ER to the cytosolic volume by the joint gating of Ca^{2+} and IP_3 , J_l denotes the leaked flux from the ER to the cytoplasm. Calcium exchanges in and out of the extracellular space are described by J_{in} and J_{out} , respectively.

The IP_3 dynamics includes the production due to PLC δ activation by the calcium released from the ER (denoted by J_{PLC}), and due to PLC β activation by the binding of glutamate $G^{(i)}$ to metabotropic receptors (denoted by J_{Glu}). The baseline steady-state concentration of IP_3 in the absence of any external input is denoted by IP_3^* , and the fraction of activated IP_3 Rs is denoted by h . The notations in the right-hand part of (5) are expressed as follows:

$$\begin{aligned} J_{\text{ER}} &= c_1 v_1 \text{Ca}^3 h^3 \text{IP}_3^3 \frac{[c_0/c_1 - (1 + 1/c_1)\text{Ca}]}{[(\text{IP}_3 + d_1)(\text{Ca} + d_5)]^3}, \\ J_{\text{pump}} &= \frac{v_3 \text{Ca}^2}{k_3^2 + \text{Ca}^2}, \\ J_l &= c_1 v_2 [c_0/c_1 - (1 + 1/c_1)\text{Ca}], \\ J_{\text{in}} &= v_5 + \frac{v_6 \text{IP}_3^2}{k_2^2 + \text{IP}_3^2}, \quad J_{\text{out}} = k_1 \text{Ca}, \\ J_{\text{PLC}} &= \frac{v_4 [\text{Ca} + (1 - \alpha)k_4]}{\text{Ca} + k_4}, \\ J_{\text{Glu}} &= \frac{\alpha_{\text{Glu}}}{1 + \exp\left(-\frac{G^{(i)} - 0.4}{0.01}\right)}. \end{aligned} \quad (6)$$

This joint dynamics of IP_3 and Ca^{2+} taken alone may provide self-sustained oscillations. When we include CICR through glutamate signaling, we get activity-evoked spontaneous Ca^{2+} oscillations mediated by IP_3 signaling. This retains physiological features observed in experimental data [36]. Parameters in (5) and (6) are described in detail and estimated empirically in [13]. In this work we use $c_0 = 2.0 \mu\text{M}$, $c_1 = 0.185$, $v_1 = 6 \text{ s}^{-1}$, $v_2 = 0.11 \text{ s}^{-1}$, $v_3 = 2.2 \mu\text{M s}^{-1}$, $v_5 = 0.025 \mu\text{M s}^{-1}$, $v_6 = 0.2 \mu\text{M s}^{-1}$, $k_1 = 0.5 \text{ s}^{-1}$, $k_2 = 1.0 \mu\text{M}$, $k_3 = 0.1 \mu\text{M}$, $a_2 = 0.14 \mu\text{M}^{-1} \text{ s}^{-1}$, $d_1 = 0.13 \mu\text{M}$, $d_2 = 1.049 \mu\text{M}$, $d_3 = 0.9434 \mu\text{M}$, $d_5 = 0.082 \mu\text{M}$, $\alpha = 0.8$, $\tau_{\text{IP}_3} = 7.143 \text{ s}$, $\text{IP}_3^* = 0.16 \mu\text{M}$, $k_4 = 1.1 \mu\text{M}$.

Parameter v_4 describes the rate of Ca^{2+} induced generation of IP_3 through PLC δ . We use two combinations of values for v_4 and α_{Glu} . In the version of the model taking into

account the bidirectional interaction between astrocytes and neurons ($\alpha_{\text{Glu}} = 9 \mu\text{M/s}$), we use $v_4 = 0.3 \mu\text{M s}^{-1}$, which corresponds to spontaneous Ca^{2+} oscillations in the CICR model [Eqs. (5) and (6)]. In the version with unidirectional coupling ($\alpha_{\text{Glu}} = 0$), we assume $v_4 = 0.5 \mu\text{M s}^{-1}$ in order to obtain Ca^{2+} self-oscillations. Note as well that the timescale for the astrocyte model is in seconds. Thus, we rescale the time units in order to match it in milliseconds for numerical integration.

The diffusive fluxes of Ca^{2+} and IP_3 molecules, which account for coupling between astrocytes by gap junctions, are denoted by $J_{\text{Ca,diff}}$ and $J_{\text{IP}_3,\text{diff}}$ and expressed as

$$\begin{aligned} J_{\text{Ca,diff}}^{(\mathbf{m})} &= d_{\text{Ca}}(\Delta\text{Ca})^{(\mathbf{m})}, \\ J_{\text{IP}_3,\text{diff}}^{(\mathbf{m})} &= d_{\text{IP}_3}(\Delta\text{IP}_3)^{(\mathbf{m})}, \end{aligned} \quad (7)$$

where the diffusion coefficients are $d_{\text{Ca}} = 0.01 \text{ s}^{-1}$ and $d_{\text{IP}_3} = 0.1 \text{ s}^{-1}$. Laplace operators $\Delta\text{Ca}^{(m,n)}$ and $\Delta\text{IP}_3^{(m,n)}$ are computed using a five-point stencil scheme with no-flux boundary conditions:

$$\begin{aligned} \Delta\text{Ca}^{(m,n)} &= \text{Ca}^{(m+1,n)} + \text{Ca}^{(m-1,n)} \\ &+ \text{Ca}^{(m,n+1)} + \text{Ca}^{(m,n-1)} - 4\text{Ca}^{(m,n)}, \end{aligned} \quad (8)$$

and same for IP_3 .

The spontaneous calcium elevations or calcium pulses trigger the release of gliotransmitters, including glutamate, back to the synaptic cleft. This has implications in the synaptic information transfer that our model incorporates through the modulation of the synaptic weight:

$$g_{\text{syn,eff}} = g_{\text{syn}}[1 + \mathcal{H}(\text{Ca}^{(\mathbf{m})} - \theta_s)g_s\text{Ca}^{(\mathbf{m})}], \quad (9)$$

where $g_{\text{syn}} = 0.04 \text{ mS/cm}^2$ is the baseline synaptic weight due to neuron-neuron communication, $\theta_s = 0.2 \mu\text{M}$ sets the minimum Ca^{2+} level to release a gliotransmitter, and \mathcal{H} is the Heaviside step function. The impact of the astrocyte in the synaptic transmission is expressed by the coupling parameter g_s . We consider that each excitatory synapse is connected to one astrocytic process forming the tripartite synapse.

It is known that astrocytes act at different levels of neuronal activity by inducing changes at individual or multiple synapses depending on the signaling pathway and location. Our model simplifies the interaction between neuron and astrocytes by just incorporating the enhancement of postsynaptic excitatory currents mediated by Ca^{2+} -dependent release of gliotransmitters (e.g., glutamate, ATP, and D-serine). In this way, we consider the effect of astrocytes through the integration of neuronal activity from glutamatergic synapses over longer timescales and feedback to postsynaptic terminals to facilitate synaptic transmission. Therefore, this model accounts for a phenomenological point of view in which we retain the effect of spontaneous activity of glial cells in the synaptic excitability. These observations include long-term potentiation in the hippocampus due to release of D-serine [37], glutamate released acting on presynaptic terminals to enhancing excitatory transmission [4], and improvement of neuronal synchrony [38].

C. Estimation of integrated information

Integrated information Φ is proposed to measure the information that the system has about its own dynamics beyond the independent contribution of its parts. For a system to exhibit integrated information, it is expected that all its possible subsystems perform their own dynamics and causally interact at the same time. Thus, highly complex patterns are possible.

Several formulations of integrated information have been proposed [39]. A promising measure is the decoder-based integrated information Φ^* [40]. It quantifies the excess of information generated by the transition dynamics of a system with respect to its nonoverlapping components, which are assumed to transition independently. In other words, for a stochastic process described by $x(t)$ with previous states $y(t) = x(t - \tau)$, Φ^* is defined as

$$\Phi^*[x, y; \pi] = I_{xy} - I_{xy;\pi}^*, \quad (10)$$

where $\pi = [M_1, M_2, \dots, M_k]$ defines the partition of the system into k independent subsystems, such that at any instant of time $x = (x_{M_1}, \dots, x_{M_k})$. I_{xy} is the mutual information between x and y [41]:

$$I_{xy} = H_x + H_y - H_{xy}. \quad (11)$$

The entropy is defined as $H_x = -\sum_x p(x) \log p(x)$ and quantifies the average information contained in x . The measure I^* denotes the mismatched decoding information, which can be understood as how much information can be extracted from a variable with a suboptimal decoding distribution [40,42]:

$$I_{xy;\pi}^* = \max_{\beta} \tilde{I}_{xy;\pi}(\beta), \quad (12)$$

where maximum over β is found using a gradient descent algorithm, and

$$\begin{aligned} \tilde{I}_{xy;\pi}(\beta) &= -\sum_x p(x) \log \sum_y p(y) q(x|y)^\beta \\ &+ \sum_{x,y} p(xy) \log q(x|y)^\beta. \end{aligned} \quad (13)$$

Here, $q(x|y)$ denotes the mismatched decoding probability distribution defined for a partition π :

$$q(x|y) = \prod_{s \in \pi} p(x_s|y_s). \quad (14)$$

Furthermore, Φ^* should be estimated using the partition π of the system at which it is minimized. This carries a high computational cost, as the calculation scales exponentially with the number of elements in the network and the number of partitions. Therefore, we apply the submodular optimization using the Queyranne's algorithm for $k = 2$ partitions, $\pi = [A, B]$, as it is the minimum case in which we can measure cause-effect information. This is a standard practice for computing integrated information and provides valid results to detect dynamical complexity [39,43].

In addition, for comparison purposes, we compute the whole-minus-sum integrated information Φ_{WMS} and mutual information between subsystems I_{AB} . Both measures provide an additional insight about the synergy and correlations in the system. The measure Φ_{WMS} provides a measure of net synergy, i.e., synergy minus redundancy [24,39,44],

$$\Phi_{\text{WMS}}[x, y; \pi = [A, B]] = I_{xy} - (I_{x_A y_A} + I_{x_B y_B}), \quad (15)$$

where $I_{x_A y_A}$ denotes the mutual information between x_A and y_A (equivalently for B). The condition $\Phi_{\text{WMS}} > 0$ implies that the system as a whole carries more information about its evolution than the sum of its parts, while $\Phi_{\text{WMS}} < 0$ implies that redundant contributions dominate.

The mutual information between subsystems I_{AB} quantifies the spatial correlation between halves of the system. That is, $I_{AB} = H_{x_A} + H_{x_B} - H_x$, by using (11).

The joint activity of $N = 6$ neurons is represented as a binary code indicating their firing pattern per each time step. Thus, the spike train of neuron i is binned by sliding a window in constant intervals $\Delta = 1$ ms using a threshold $V_\theta = -40$ mV. In this way, for every neuron if a spike is found at $[t, t + \Delta]$, i.e., $V^{(i)} > V_\theta$, we set the state as $x_i = 1$, otherwise, $x_i = 0$. The state of the population of neurons x is defined by its joint activity at any instant of time, which corresponds to a binary array of N bits. The probability associated to each state is obtained by its empirical frequency distribution. Estimation of information-theoretic measures were obtained through the ‘‘practical PHI toolbox’’ [26,40,43,45] ensuring convergent behavior.

D. Measures of synchronization

The degree of synchronization of the neurons is represented by an order parameter \bar{r} that quantifies the phase dispersion of the spike trains. The instantaneous phase can be described as

$$\theta(t) = 2\pi k + 2\pi \frac{t - t_k}{t_{k+1} - t_k}, \quad (16)$$

where t_k is the firing time of a neuron. In other words, the change of phase between two firing times carries an increase of 2π , and for $t \in [t_k, t_{k+1}]$ the phase increases linearly. The instantaneous synchronization $r(t)$ is defined by

$$r(t) = \left| \frac{1}{N} \sum_{j=1}^N e^{i\theta_j} \right|, \quad (17)$$

where θ_j denotes the instantaneous phase for each neuron $j = 1, \dots, N$. The order parameter $\bar{r} = \langle r(t) \rangle$ quantifies the average coherence across time of Eq. (17). According to (17), a completely asynchronous behavior implies $\bar{r} = 0$, while for full synchronization we get $\bar{r} = 1$. This measure quantifies the interaction between individual neurons. We report $r(t)$ after binning the spike trains with a window of 10 ms at constant intervals [46]. Similar results were obtained for lower sizes.

III. RESULTS

We applied the fourth-order Runge-Kutta method to solve Eqs. (1) and (5) on networks described above. For each network we stimulate the neurons with a Poisson pulse train with rate $\lambda = 20$ Hz, while the coupling parameter g_s is varied. We consider both unidirectional and bidirectional neuron-astrocyte communication as described previously in Sec. II B. For the second set of simulations, we fix the coupling parameter and vary the frequency λ . Here, the excitatory network has all-to-all coupling with $g_s = 2.5$ (considering just unidirectional feedback from astrocytes), while the network with an inhibitory neuron and nearest-neighbor coupling is set at

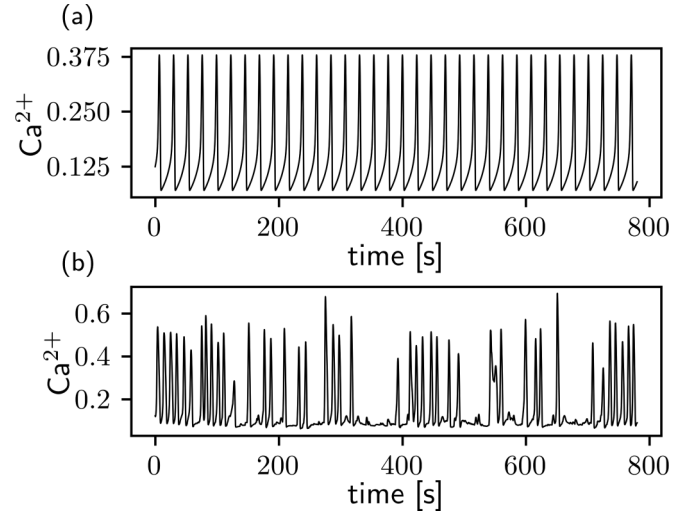


FIG. 2. Simulated Ca^{2+} patterns in an astrocyte obtained for (a) unidirectional feedback $J_{\text{Glu}} = 0$, $v_4 = 0.5 \mu\text{M s}^{-1}$ and (b) bidirectional neuron-astrocyte coupling $J_{\text{Glu}} > 0$, $v_4 = 0.3 \mu\text{M s}^{-1}$. The neural network used is exc-nns with $g_s = 3.42$.

$g_s = 7.5$ (by including unidirectional and bidirectional communication). The time length for each simulation is 1500 s with a time step $\Delta t = 0.09$ ms. First 500 s were discarded to avoid effects from transient states. Next, we binarize the spike trains using a bin width T set to 1 ms, from where we compute the information-theoretic measures. Estimations of integrated information show convergence for increased length of time series for this timescale.

A. Collective behavior in neuron-astrocyte networks

When we just consider unidirectional feedback from astrocytes, there are self-sustained regular Ca^{2+} oscillations [Fig. 2(a)]. However, when we allow neuron-astrocyte feedback there is an interplay between the time-dependent glutamate signals released from the synaptic activity and the level of Ca^{2+} stimulated throughout the CICR process [Fig. 2(b)]. It is well known that Ca^{2+} dynamics can undergo different bifurcations in response to feedback from neurons and biological parameters [47], so different modes of encoding of stimuli are possible. In this paper, we emphasize the effect of the bidirectional feedback between spontaneous calcium oscillations and neuronal activity on the integration of the stimuli in the population coding.

First, our simulations indicate small spontaneous oscillations for typical Ca^{2+} and IP_3 resting concentrations using $v_4 = 0.3 \mu\text{M s}^{-1}$. As we increase the coupling parameter g_s , Ca^{2+} pulslike fluctuations arise with mixed amplitude and frequency modulation (AFM) due to the influence of glutamate released by the spike trains. For example, Fig. 2 considers two cases associated with neuron-astrocyte communication: (a) regular and (b) spontaneous oscillations.

When bidirectional communication between neurons and astrocytes is set, the frequency of spontaneous calcium oscillations increases with the synaptic activity. As a consequence, there is positive reinforcement between both. This regime is in agreement with experimental observations [36,48,49].

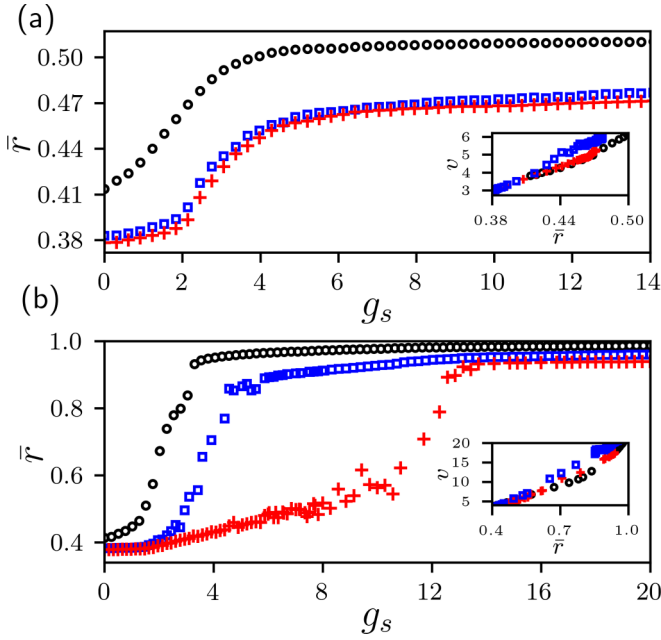


FIG. 3. Order parameter \bar{r} as the coupling g_s is varied. Inset: dependence of the average firing rate v (s^{-1}) of the population of neurons upon \bar{r} . Plots are shown for (a) unidirectional and (b) bidirectional communication. Each marker represents a network architecture: black open circle [exc-full, Fig. 1(a)], blue open square [exc-nns, Fig. 1(b)], and red plus [inh-nns, Fig. 1(c)].

Further stimulation through g_s induces a transition to an upper fixed point, in which Ca^{2+} abruptly converges towards stable (constant) concentration levels. This state corresponds to a sustained plateau of Ca^{2+} , which in practical situations triggers only a single Ca^{2+} pulse. Therefore, this dynamical regime is not biologically relevant for our analysis.

We next compute the synchronization between neurons due to the effect of astrocytes. In Fig. 3(a) the order parameter \bar{r} transitions to a limit value (around $1.8 \leq g_s \leq 4.8$). Next, it remains practically bounded by $\bar{r} \simeq 0.51$. This rise is consistent with the fact that astrocytes are forcing the assemblies with the same oscillatory input [Fig. 2(a)]. This creates a periodic increase in the firing rate as Ca^{2+} peaks at the same times for all neurons. Nonetheless, as we allow feedback from the glutamate signals to astrocytes \bar{r} outperforms reaching nearly full synchronization [Fig. 3(b)]. The transition points to high \bar{r} (around $1.8 \leq g_s \leq 4.8$ for exc-full and exc-nns, and $g_s \simeq 12.5$ for inh-nns) are clearly dependent on the network architectures and balance between excitatory and inhibitory responses.

The observed behavior in excitatory networks shows that synchronization is favored for all-to-all coupling due to the high integration in the network, followed by the nearest-neighbor coupling. The inhibitory neuron leads the transition to synchronization at higher g_s with respect to the excitatory case. This is because the inhibitory synapse reduces the firing frequency of the neighboring excitatory neurons. As a consequence, the calcium events associated to those synapses are less frequent. Thus, higher g_s is needed to compensate this reduction in astrocytic feedback. In our modeling, this effect has the benefit of modulating the potentiation of excitatory

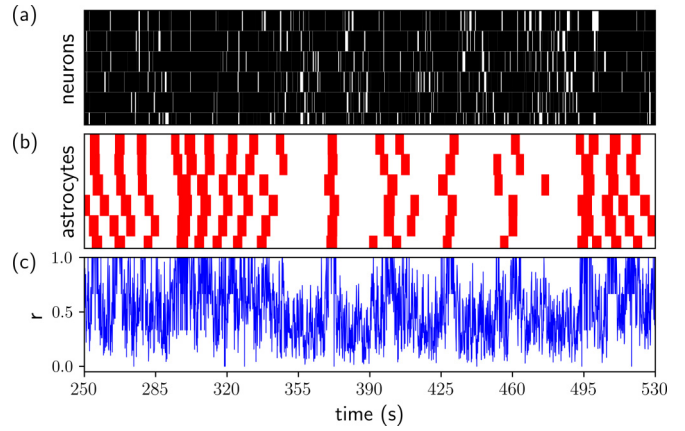


FIG. 4. Raster plots of (a) neuronal and (b) astrocytic activity at $g_s = 3.4$ and $\lambda = 20$ Hz with bidirectional coupling. Plots correspond to an excitatory network with all-to-all coupling [exc-full, Fig. 1(a)]. Bottom figure (c) shows the instantaneous synchronization of the neurons defined according to Eq. (17).

currents mediated by the astrocytes. However, from the results presented here, the role of bidirectional feedback suggests an increased self-organization for all the networks. This hints about the role of astrocytes as regulators of bursting of neuronal populations [35,50,51].

These results suggest that astrocytes integrate neural signals through the IP_3 transduction and respond in the form of pulses allowing dynamical coordination in the neurons. For instance, in Fig. 4 we present a raster plot for an excitatory network with all-to-all coupling, exc-full. As the neurons produce glutamate the IP_3 encodes the state of the neuron in a slower timescale and activates calcium bursts and pulses. This allows episodes of high synchronization in the whole network as expressed by r . As we will discuss in the next section, this has implications in the information processing mechanism of the neural assemblies.

B. Information processing in neuron-astrocyte communication

The obtained dependencies of the integrated information Φ^* with different values of time delay τ and coupling values g_s are shown on Fig. 5. The results in the upper row (a) correspond to the case of unidirectional feedback from astrocytes, and in the lower row (b) to bidirectional neuron-astrocyte communication.

The comparison between Figs. 5(a) and 5(b) shows that Φ^* is significantly enhanced for all the network architectures reported with neuron-astrocyte feedback. Next, the networks exhibit strong peaks at synaptically relevant timescales $\tau = 2$ and 20 ms. These results are arguably related to the spiking-bursting dynamics due to neuron-neuron interactions and input noise. In particular, the first peak is an indication of the substantial correlation and integration of short-term information from past states of the system, while the second one reflects the train pulse duration of 10 ms and correlations between firing patterns.

An instance of such is shown in Fig. 6, corresponding to an excitatory network with all-to-all coupling, exc-full. Note that at $g_s = 0$ there is positive Φ^* attributable to neuron-neuron

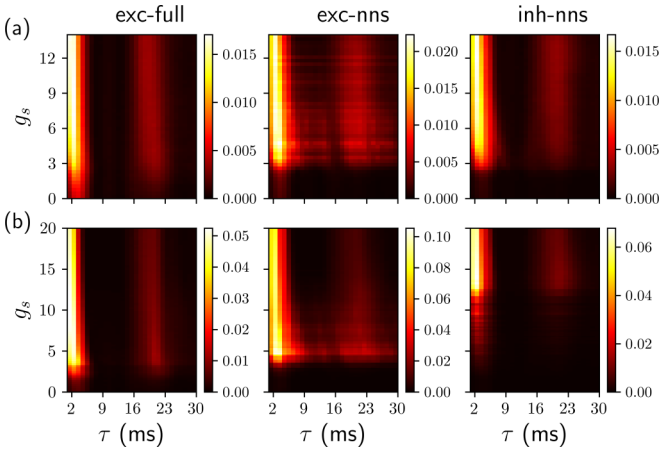


FIG. 5. Integrated information Φ^* for different coupling values g_s and timescales τ . Each column indicates the network under consideration (shown in Fig. 1). Top row (a) shows the results for the unidirectional feedback from astrocytes and (b) the bidirectional neuron-astrocyte communication. Bright region of the heat plots corresponds to maximal Φ^* around 2 ms and the shaded region around 20 ms indicates its second peak. Both peaks emerge as g_s grows as described in the text.

interactions. Initial peaks are sharpened through larger g_s defining two timescales with greater Φ^* . Again, higher integration of information is observed when neuron-astrocyte interaction is considered.

To study further the dependency of Φ^* upon the coupling g_s , we fix $\tau = 2$ ms. Figures 7(a) and 7(d) show the integrated information for unidirectional and bidirectional communication, respectively. Greater values of Φ^* are observed in all cases when neuron-astrocyte feedback is present. This suggests that bidirectional communication overall increases the amount of information that the system holds about its own dynamics, at short timescales with respect to the contribution of its parts.

In addition, we observe that different networks undergo a transition to high Φ^* with varied g_s similarly to the behavior of the synchronization parameter \bar{r} observed in Fig. 3. For unidirectional coupling there is a sigmoid transition followed by a plateau. In our simulations this is bounded by $\Phi^* \simeq 0.022$ [Fig. 7(a)]. For bidirectional coupling, Φ^* peaks in the transition regime [Fig. 7(d)] and then shrinks as Ca^{2+} concentration

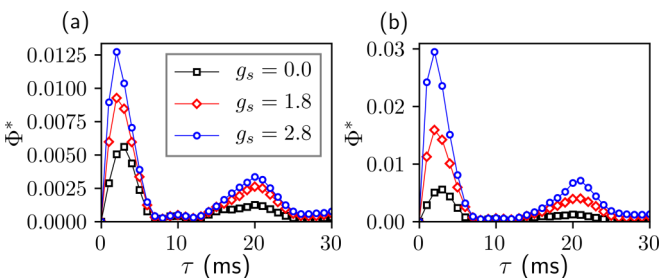


FIG. 6. Integrated information Φ^* for different coupling values g_s and varied timescales τ . The network architecture corresponds to exc-full [Fig. 1(a)] for (a) unidirectional and (b) bidirectional coupling.

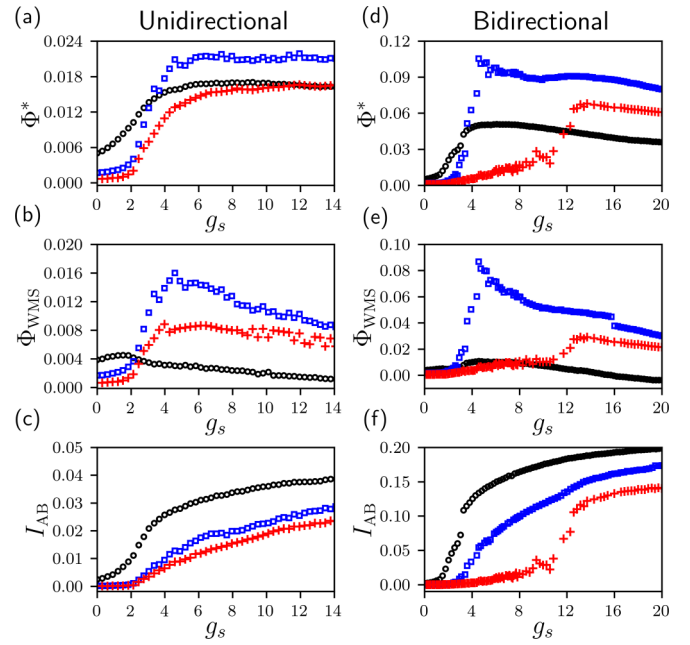


FIG. 7. Measures Φ^* (integrated information), Φ_{WMS} (net synergy), and I_{AB} (mutual information). Left column: (a)–(c) indicate values associated with unidirectional feedback from astrocytes. Right column: (d)–(f) show values for the bidirectional neuron-astrocyte communication. Φ^* and Φ_{WMS} are reported at $\tau = 2$ ms. Legends are defined as in Fig. 3.

becomes permanently high. Here, Φ^* can be up to five times higher than in the unidirectional case.

The excitatory network with all-to-all coupling exc-full transitions first followed by the nearest-neighbor one exc-nns. In a the long run, for both cases the nearest-neighbor assembly has larger Φ^* . These results are a consequence of the heterogeneous design of exc-nns, which outputs balanced firing patterns as each spike is just dependent of the nearest structural neighbors. By adding inhibition, as in inh-nns, the transition regime is right shifted to higher g_s . This is not surprising as the inhibition of excitatory synapses reduces the excitatory transmission from neurons to astrocytes and, ultimately, affects the event rate of Ca^{2+} pulses, as already discussed. As a consequence, this widens the observed transition of Φ^* and \bar{r} . After Ca^{2+} oscillations are replaced by a regime where Ca^{2+} concentration is permanently high, all the architectures transition to higher degrees of synchronization and there is a decline in Φ^* , which is associated with an excess correlation.

To further support our hypothesis that the integrated information is enhanced through bidirectional coupling, we compute the net synergy Φ_{WMS} and mutual information I_{AB} . This is in order to investigate the relationship between our observations in Sec. III A with the behavior of these measures. As shown in Fig. 7, Φ_{WMS} and I_{AB} mirror the transition of \bar{r} (in turn, the dynamical transition of the Ca^{2+} dynamics) as well. We note the following when neurons and astrocytes interact: the overall synergy and correlation increase with g_s , and the net synergy peaks just at the transition point but drops afterwards, meanwhile, the correlation increases continuously with g_s . This implies that Φ^* is maximized when the correlation

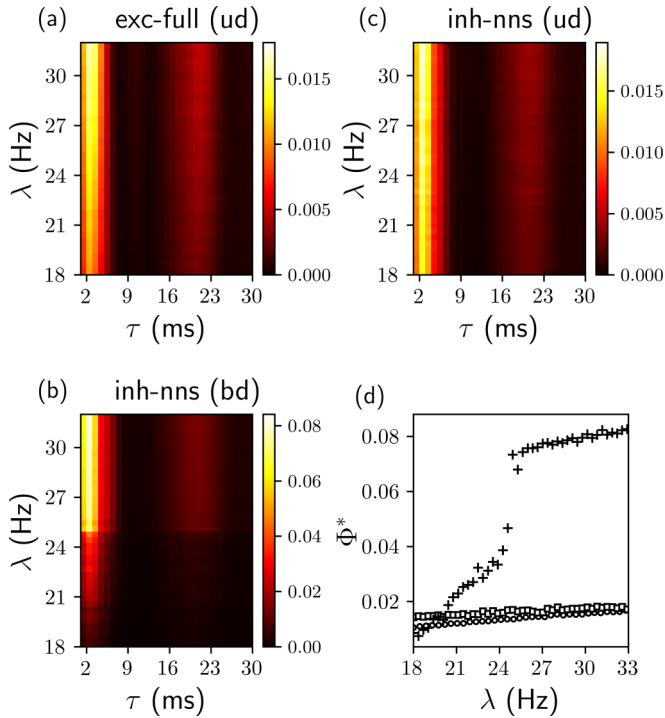


FIG. 8. (a)–(c) Integrated information Φ^* for different stimulation frequencies λ and timescales τ : (a) exc-full network [Fig. 1(a)] with fixed coupling $g_s = 2.5$ and (b), (c) inh-nns network [Fig. 1(c)] with $g_s = 7.5$. Unidirectional feedback is denoted by (ud) and bidirectional (bd). (d) Φ^* for fixed $\tau = 2$ ms and varied λ . Markers: exc-full, open circle; inh-nns (ud), open square; and inh-nns (bd), plus. (a)–(c) Bright region of the heat plots corresponds to maximal Φ^* around 2 ms and the shaded region around 20 ms indicates its second peak. Both peaks increase with λ as described in the text.

among neurons is balanced with the independent dynamics of its constituents. As g_s grows, redundancy counterbalances the synergy in the system due to excess correlation and decreases Φ^* . This is a consequence of the dynamical transition to permanent high Ca^{2+} concentration, affecting equally all the neurons in the network.

If we relate Φ^* with I_{AB} for each network, we can observe that exc-full has the highest degree of correlation (integration) but the lowest integrated information, and redundancy dominates for increased neuron-astrocyte coupling. On the contrary, inh-nns shows the lowest degree of correlation but there are higher synergistic effects, which provide a higher contribution of integration of information. However, for intermediate values of correlation, when we compare the three networks, exc-nns has the highest integrated information.

Observe that the synergy and correlation are rather small in the unidirectional case. These results highlight the complex interplay between neural connectivity and neuron-astrocytic interactions to get optimal population coding. Indeed, it is reported that a balance between excess correlation and desynchronization supports information processing in neurons [52–54], and this has implications in higher order cognitive and behavioral processes. Thus, both measures Φ_{WMS} and I_{AB} are also dominant for the bidirectional coupling. This implies that the system undergoes enhanced integration but at the

same time, the generated information is less redundant with respect to the contribution from its components. This confirms that integrated information is favored when we introduce a positive feedback between neurons and astrocytes and is maximized at the transition regime between spontaneous activity to a high stable equilibrium.

Finally, we consider the impact of the input noise on the integrated information values. Increased frequency does not appear to change the general behavior of Φ^* discussed up to this point. For the unidirectional case, Figs. 8(a) and 8(c), the integrated information peaks at $\tau = 2$ and 20 ms, and remains steady for the range of frequencies considered in this paper. In contrast, neuron-astrocyte communication shows a sudden transition around $\lambda \simeq 24$ Hz [Fig. 8(b)]. At $\tau = 2$ ms the integrated information grows linearly with λ in the unidirectional case. However, the effects are negligible to provide any substantial change. In contrast, the bidirectional case shows a rapid increase that sets after transitioning as described [Fig. 8(d)]. Simulations show that this point corresponds to the switch between AFM spontaneous Ca^{2+} activity and a higher stable state. This result confirms again that Φ^* increases at the transition between dynamical regimes.

IV. DISCUSSIONS AND CONCLUSIONS

We investigated the behavior of integrated information in glutamate-mediated neuron-astrocyte interaction. Different neural networks connected to a network of astrocytes were stimulated with an external uncorrelated input iterating over different network assemblies, noise levels, and dynamical regimes. Integrated information was quantified in two scenarios: (1) astrocyte-to-neuron one-way influence and (2) bidirectional neuron-astrocyte mutual interaction.

It is found that Φ^* significantly increases with bidirectional communication, a condition in which the astrocytes underpin dynamic synchronization in the neurons. Further analysis through the calculation of mutual information and net synergy corroborated that integrated information in these systems is maximized when there is a balance between excess correlation and spontaneous spiking activity. This condition is satisfied near criticality previously to reach a high concentration state. Also, consistently with previous results, our simulations show that the encoding of information in these systems is more efficient than its individual contributions when neurons hold a heterogeneous connectivity. It allows local interactions with global integration of information, rather than a homogeneous one.

Note that, due to our finite-time estimate of information, we do not capture the full repertoire of calcium events for the regime under consideration. Generally, calcium oscillations may display complex patterns with varied amplitude, shape, and frequency as a mechanism of information encoding. The effect of calcium events variation upon integrated information requires further investigation. Nevertheless, while this oscillatory diversity is not taken into account, we observe that at a synaptic timescale integrated information is higher due to this neuron-astrocyte communication.

These results support the conjecture that the IP_3 transduction of glutamate patterns and cross coupling between the IP_3 and Ca^{2+} signals further contribute to the emergence of

integrated information in neuron-astrocyte networks. In other words, this coupling may favor flexible coordination among the neuronal patterns yielding more information from the population than the sum of its parts.

Although validation is needed from experimental data and conclusions were derived from simulations in a reduced model, the aim of this paper is to investigate the relationship between a well-known signaling pathway observed in neuron-astrocyte communication and the information processing in neuronal populations. Our analysis retains the main physiological features of this pathway, and suggests at a possible link with the emergence of integration of information.

From previous results it is shown that Φ^* is favored at the boundary areas between random and ordered phases [29,55,56]. For example, this situation takes place during metastable conditions and phase transitions in self-organized criticality. In this sense, criticality as a working condition in the brain and metastability are two possible ways in which this measure may grow given that there is a propagation of neural signals in a coordinated manner among multiple neuronal populations. Experimental results relying on the balance of excitation and inhibition in cortical cultures confirm the role of criticality for wakefulness [57–59] using neuronal avalanche metrics. Likewise, highly metastable systems, such as chimera states, are thought to form a basis of cognition [60,61]. These scenarios provide the brain functional specialization and functional integration, which may lead to the conscious experience and higher-order processes.

In our modeling approach, we relate the emergence of a large Φ^* to the switch of semisynchronized states allowing

an optimal representational capacity of the network while minimizing redundant contributions. In such a case, the neural network has a balanced spread of input excitability. As said, our observations indicate this balance takes place in the transition from a random to an ordered phase near the edge of criticality. This is in line with results that suggest that astrocytes induce activity-dependent neuronal synchronization through complex bifurcation dynamics. However, it is equally plausible that in larger systems, astrocytes mediate synchronization between groups of neurons to propagate spatiotemporal patterns across different areas through unstable dynamics. Previous works suggest that conscious processing may relate with the integration of neural signals coming to astrocytes inducing Ca^{2+} release when the unstable state of IP_3 activity reaches a fixed point [62]. It is also shown that astrocytes can switch synaptic plasticity between depression and potentiation in groups of synapses for learning tasks [63]. Further research is needed to assess this question. As of late, we are currently developing a large-scale model to understand the switching coordination provided in an astrocyte-neuron network in the context of information processing.

ACKNOWLEDGMENTS

L.A. acknowledges CONACYT for his doctoral scholarship to conclude this work. A.Z. acknowledges support from MRC Grant No. MR/R02524X/1. We acknowledge support by the grant of the Ministry of Education and Science of the Russian Federation Agreement Grant No. 075-15-2020-808.

-
- [1] T. Fellin, *J. Neurochem.* **108**, 533 (2009).
 - [2] C. Agulhon, J. Petravicz, A. B. McMullen, E. J. Sweger, S. K. Minton, S. R. Taves, K. B. Casper, T. A. Fiacco, and K. D. McCarthy, *Neuron* **59**, 932 (2008).
 - [3] P. Jourdain, L. H. Bergersen, K. Bhaukaurally, P. Bezzi, M. Santello, M. Domercq, C. Matute, F. Tonello, V. Gundersen, and A. Volterra, *Nat. Neurosci.* **10**, 331 (2007).
 - [4] G. Perea and A. Araque, *J. Physiol. Paris* **96**, 199 (2003).
 - [5] G. Perea, M. Navarrete, and A. Araque, *Trends Neurosci.* **32**, 421 (2009).
 - [6] R. Min, M. Santello, and T. Nevian, *Front. Comput. Neurosci.* **6**, 93 (2012).
 - [7] J. T. Porter and K. D. McCarthy, *J. Neurosci.* **16**, 5073 (1996).
 - [8] V. Parpura, T. A. Basarsky, F. Liu, K. Jeftinija, S. Jeftinija, and P. G. Haydon, *Nature (London)* **369**, 744 (1994).
 - [9] A. Araque, V. Purpura, R. P. Sanzgiri, and P. G. Haydon, *Trends Neurosci.* **22**, 208 (1999).
 - [10] J. J. Wade, L. J. McDaid, J. Harkin, C. Vincenzo, and J. A. S. Kelso, *PLoS One* **6**, e29445 (2011).
 - [11] S. Y. Gordleeva, S. A. Lebedev, M. A. Romyantseva, and V. B. Kazantseva, *JETP Lett.* **107**, 440 (2018).
 - [12] M. De Pitta, V. Volman, H. Berry, and E. Ben-Jacob, *PLoS Comput. Biol.* **7**, e1002293 (2011).
 - [13] G. Ullah, P. Jung, and A. H. Cornell-Bell, *Cell Calcium* **39**, 197 (2019).
 - [14] G. W. De Young and J. Keizer, *Proc. Natl. Acad. Sci. USA* **89**, 9895 (1992).
 - [15] M. De Pitta, M. Goldberg, V. Volman, H. Berry, and E. Ben-Jacob, *J. Biol. Phys.* **36**, 221 (2010).
 - [16] E. V. Pankratova, A. I. Kalyakulina, S. V. Stasenkov, S. Y. Gordleeva, I. A. Lazarevich, and V. B. Kazantsev, *Nonlinear Dyn.* **97**, 647 (2019).
 - [17] A. Pereira and F. A. Furlan, *Prog. Neurobiol.* **92**, 405 (2010).
 - [18] A. Engel, K. J. Friston, J. A. S. Kelso, P. Konig, I. Kovacs, A. MacDonald, E. Miller, W. Phillips, S. Silverstein, C. Tallon-Baudry, J. Triesch, and P. Uhlhaas, *Coordination in behavior and cognition*, in *Dynamic Coordination in the Brain: From Neurons to Mind*, Vol. 5 (MIT Press, Cambridge, MA, 2010).
 - [19] S. Y. Gordleeva, A. V. Ermolaeva, I. A. Kastalskiy, and V. B. Kazantsev, *Front. Physiol.* **10**, 294 (2019).
 - [20] G. Tononi, O. Sporns, and G. Edelman, *Proc. Natl. Acad. Sci. USA* **91**, 5033 (2003).
 - [21] D. Balduzzi and G. Tononi, *PLoS Comput. Biol.* **4**, e1000091 (2008).
 - [22] M. Oizumi, L. Albantakis, and G. Tononi, *PLoS Comput. Biol.* **10**, e1003588 (2014).
 - [23] H. Kim, A. G. Hudetz, J. Lee, G. A. Mashour, and U. Lee, *Front. Hum. Neurosci.* **12**, 42 (2018).
 - [24] A. K. Seth, A. B. Barrett, and L. Barnett, *Philos. Trans. R. Soc., A* **369**, 3748 (2011).

- [25] J. R. Isler, R. I. Stark, P. G. Grieve, M. G. Welch, and M. M. Myers, *PLoS One* **13**, e0206237 (2018).
- [26] M. Oizumi, N. Tsuchiya, and S. Amari, *Proc. Natl. Acad. Sci. USA* **113**, 14817 (2016).
- [27] M. Tegmark, *PLoS Comput. Biol.* **12**, e1005123 (2016).
- [28] O. Kanakov, S. Gordleeva, A. Ermolaeva, S. Jalan, and A. Zaikin, *Phys. Rev. E* **99**, 012418 (2019).
- [29] L. Abrego and A. Zaikin, *Entropy* **21**, 382 (2019).
- [30] S. Gordleeva, S. Stasenko, A. Semyanov, A. Dityatev, and V. Kazantsev, *Front. Comput. Neurosci.* **6**, 92 (2012).
- [31] A. L. Hodgkin and A. F. Huxley, *J. Physiol.* **117**, 500 (1952).
- [32] V. B. Kazantsev and S. Y. Asatryan, *Phys. Rev. E* **84**, 031913 (2011).
- [33] P. M. Esir, S. Y. Gordleeva, A. Y. Simonov, A. N. Pisarchik, and V. B. Kazantsev, *Phys. Rev. E* **98**, 052401 (2018).
- [34] A. Araque, G. Carmignoto, P. G. Haydon, S. H. Oliet, R. Robitaille, and A. Volterra, *Neuron* **81**, 728 (2014).
- [35] S. Y. Makovkin, I. V. Shkerin, S. Y. Gordleeva, and M. V. Ivanchenko, *Chaos, Soliton Fractons* **138**, 109951 (2020).
- [36] V. Parpura, *Glutamate-mediated bi-directional signaling between neurons and astrocytes*, *Glial-Neuronal Signaling* (Kluwer Academic, Amsterdam, 2004).
- [37] C. Henneberger, T. Papouin, S. H. Oliet, and D. A. Rusakov, *Nature (London)* **463**, 232 (2010).
- [38] T. Fellin, O. Pascual, S. Gobbo, T. Pozzan, P. G. Haydon, and G. Carmignoto, *Neuron* **43**, 729 (2004).
- [39] P. A. Mediano, A. K. Seth, and A. B. Barrett, *Entropy* **21**, 17 (2019).
- [40] M. Oizumi, S. Amari, T. Yanagawa, N. Fujii, and N. Tsuchiya, *PLoS Comput. Biol.* **12**, e1004654 (2016).
- [41] T. Cover, *Elements of Information Theory* (Wiley, Hoboken, NJ, 2012).
- [42] M. Oizumi, T. Ishii, K. Ishibashi, T. Hosoya, and M. Okada, *J. Neurosci.* **30**, 4815 (2010).
- [43] S. Hidaka and M. Oizumi, *PLoS One* **13**, e0201126 (2018).
- [44] V. Griffith and C. Koch, Quantifying synergistic mutual information, in *Guided Self-Organization: Inception*, edited by M. Prokopenko (Springer, Berlin, 2014), pp. 159–190.
- [45] J. Kitazono, R. Kanai, and M. Oizumi, *Entropy* **20**, 173 (2018).
- [46] A. R. C. Paiva, I. Park, and J. C. Principe, Inner products for representation and learning in the spike train domain, in *Statistical Signal Processing for Neuroscience and Neurotechnology*, edited by K. G. Oweiss (Academic, Oxford, 2010), pp. 265–309.
- [47] V. Matrosov, S. Gordleeva, N. Boldyreva, E. Ben-Jacob, and V. Kazantsev, *Comput. Gliosci.* **1**, 151 (2018).
- [48] X. Wang, N. Lou, Q. Xu, G. Tian, W. Peng, X. Han, J. Kang, T. Takano, and M. Nedergaard, *Nat. Neurosci.* **9**, 816 (2006).
- [49] A. Cornell-Bell, S. Finkbeiner, M. Cooper, and S. Smith, *Science* **247**, 470 (1990).
- [50] K. Lenk, E. Satu vuori, J. Lallouette, A. Ladron-de Guevara, H. Berry, and J. A. K. Hyttinen, *Front. Comput. Neurosci.* **13**, 92 (2019).
- [51] H. S. Lee, A. Ghetti, A. Pinto-Duarte, X. Wang, G. Dzieczapolski, F. Galimi, S. Huitron-Resendiz, J. C. Piña-Crespo, A. J. Roberts, I. M. Verma, T. J. Sejnowski, and S. F. Heinemann, *Proc. Natl. Acad. Sci. USA* **111**, E3343 (2014).
- [52] B. Averbeck, P. E. Latham, and A. Pouget, *Nat. Rev. Neurosci.* **7**, 358 (2006).
- [53] O. B. Mayo, L. Berdondini, and D. T. De Pietri, *Methods Mol. Biol.* **1938**, 131 (2019).
- [54] D. A. Gutnisky and V. Dragoi, *Nature (London)* **452**, 220 (2008).
- [55] P. A. Mediano, J. C. Farah, and M. Shanahan, [arXiv:1606.08313](https://arxiv.org/abs/1606.08313).
- [56] H. Mori and M. Oizumi, Information integration in a globally coupled chaotic system, in *the 2018 Conference on Artificial Life: A Hybrid of the European Conference on Artificial Life (ECAL) and the International Conference on the Synthesis and Simulation of Living Systems (ALIFE)* (MIT Press, Cambridge, MA, 2018), pp. 384–385.
- [57] J. M. Beggs and D. Plenz, *J. Neurosci.* **23**, 11167 (2003).
- [58] W. L. Shew, H. Yang, T. Petermann, R. Roy, and D. Plenz, *J. Neurosci.* **29**, 5595 (2009).
- [59] W. Shew, H. Yang, S. Yu, R. Roy, and D. Plenz, *J. Neurosci.* **31**, 55 (2011).
- [60] E. Tognoli and J. A. K. Scott, *Neuron* **81**, 35 (2014).
- [61] K. Bansal, J. O. Garcia, S. H. Tompson, T. Verstynen, J. M. Vettel, and S. F. Muldoon, *Sci. Adv.* **5**, eaau8535 (2019).
- [62] A. Pereira Jr. and F. A. Furlan, *J. Biol. Phys.* **35**, 465 (2009).
- [63] M. De Pitta and N. Brunel, *Neural Plast.* **2016**, 7607924 (2016).